

# Electron-enhanced SiO<sub>2</sub> atomic layer deposition at 35 °C using disilane and ozone or water as reactants

Cite as: J. Vac. Sci. Technol. A 41, 042404 (2023); doi: 10.1116/6.0002726

Submitted: 27 March 2023 · Accepted: 12 May 2023 ·

Published Online: 20 June 2023



View Online



Export Citation



CrossMark

Jonas C. Gertsch,<sup>1</sup>  Zachary C. Sobell,<sup>1</sup>  Andrew S. Cavanagh,<sup>1</sup>  Harsono Simka,<sup>2</sup> and Steven M. George<sup>1</sup> 

## AFFILIATIONS

<sup>1</sup>Department of Chemistry, University of Colorado, Boulder, Colorado, 80309

<sup>2</sup>Logic Pathfinding Lab, Samsung Semiconductor, Inc., San Jose, California, 95134

**Note:** This paper is part of the 2024 Special Topic Collection on Atomic Layer Deposition (ALD).

## ABSTRACT

Electrons can enhance SiO<sub>2</sub> atomic layer deposition (ALD) at low temperatures using disilane (Si<sub>2</sub>H<sub>6</sub>) and either ozone (O<sub>3</sub>/O<sub>2</sub>) or water (H<sub>2</sub>O) as reactants. SiO<sub>2</sub> electron-enhanced ALD (EE-ALD) was demonstrated at 35 °C by exposing the sample to sequential electron, oxygen reactant, and Si<sub>2</sub>H<sub>6</sub> exposures. The reaction sequence was electron beam exposure for 3 s, purge for 5 s, O<sub>3</sub>/O<sub>2</sub> or H<sub>2</sub>O exposure at 0.5–1.0 Torr for 3 s, purge for 10 s, Si<sub>2</sub>H<sub>6</sub> exposure at 100 mTorr for 1 s, and purge for 15 s. The electron exposure was an electron current of ~150 mA for 3 s. The electrons were produced by a hollow cathode plasma electron source typically operating with a grid bias of ~−300 V. These electrons could irradiate a sample area of ~2 × 2 cm<sup>2</sup>. *In situ* spectroscopic ellipsometry measurements determined that SiO<sub>2</sub> EE-ALD films nucleated rapidly and deposited linearly versus number of EE-ALD cycles. The SiO<sub>2</sub> EE-ALD growth rate was 0.89 Å/cycle using O<sub>3</sub>/O<sub>2</sub> and 0.88 Å/cycle using H<sub>2</sub>O. The SiO<sub>2</sub> growth rate was also self-limiting at higher electron and Si<sub>2</sub>H<sub>6</sub> exposures. In addition, SiO<sub>2</sub> EE-ALD films were grown by changing the reaction sequence or codosing the electrons with the oxygen reactant. The SiO<sub>2</sub> EE-ALD films could be grown on conducting silicon wafers or insulating SiO<sub>2</sub> films. SiO<sub>2</sub> EE-ALD is believed to be possible on insulating SiO<sub>2</sub> films because the secondary electron yield for SiO<sub>2</sub> at electron energies of ~100–300 eV is greater than unity. Under these conditions, the SiO<sub>2</sub> film charges positive during electron exposure and then pulls back secondary electrons to maintain charge neutrality. The SiO<sub>2</sub> EE-ALD films had properties that were comparable with thermal SiO<sub>2</sub> oxides. The refractive indices of the SiO<sub>2</sub> EE-ALD films were similar at  $n = 1.44 \pm 0.02$  for various process conditions and equivalent to the refractive index of a wet thermal SiO<sub>2</sub> oxide film. In addition, all the SiO<sub>2</sub> EE-ALD films yielded etch rates in dilute buffered oxide etch solution that were only slightly higher than the etch rate of a thermal SiO<sub>2</sub> oxide film. SiO<sub>2</sub> EE-ALD should be useful to deposit high-quality SiO<sub>2</sub> films for various applications at low temperatures.

Published under an exclusive license by the AVS. <https://doi.org/10.1116/6.0002726>

## I. INTRODUCTION

Electrons can provide a nonthermal means to enhance thin film growth at low temperatures. The interaction between electrons and surface species can lead to desorption of surface species via electron stimulated desorption (ESD).<sup>1</sup> This ESD can create reactive sites on the surface that facilitate adsorption of reactants and thin film growth.<sup>2</sup> Electrons can also collide with gas phase species and induce dissociation. This dissociation creates radical species that can react with the surface and promote thin film growth.<sup>3</sup>

Most of the work on electron-enhanced growth has concentrated on focused electron beams.<sup>4,5</sup> The field of focused electron beam induced deposition (FEBID) has developed direct write

methods for patterned deposition and nanostructure fabrication.<sup>4,5</sup>

In contrast, there are very few reports of using broad electron beams for thin film growth over large surface areas. Although plasma atomic layer deposition (ALD) is widely employed for thin film growth,<sup>6</sup> there have been only a few investigations on electron-enhanced ALD (EE-ALD).

EE-ALD has been demonstrated for GaN, Si, BN, and Co film growth. GaN is a binary compound and GaN EE-ALD employed Ga(CH<sub>3</sub>)<sub>3</sub>, NH<sub>3</sub>, and electrons as the reactants.<sup>7</sup> Si is a single element, and Si EE-ALD used only Si<sub>2</sub>H<sub>6</sub> and electrons as the reactants.<sup>8</sup> Although BN is a binary compound, BN EE-ALD utilized the single-source precursor borazine (B<sub>3</sub>N<sub>3</sub>H<sub>6</sub>) and electrons as the

reactants.<sup>9</sup> Co is a single-element film and Co EE-ALD employed  $\text{CoNO}(\text{CO})_3$  and electrons as the reactants.<sup>10</sup> These films were all grown at room temperature using electrons with an energy of 75–175 eV from an electron gun.<sup>7–10</sup> The electron gun could only provide limited electron currents of  $\leq 100 \mu\text{A}$  and required low pressures of  $\leq 10^{-7}$  Torr.<sup>7–10</sup>

New electron sources have been developed for EE-ALD using a hollow cathode plasma electron source (HC-PES).<sup>11</sup> The HC-PES can deliver much higher electron currents of  $>100 \text{ mA}$  and can operate at higher chamber pressures of  $\sim 5 \text{ mTorr}$ .<sup>11</sup> Co EE-ALD was recently demonstrated using the HC-PES with shorter cycle times and larger growth areas compared with the earlier Co EE-ALD studies based on the electron gun.<sup>10,11</sup> In addition, TiN EE-ALD was recently accomplished using tetrakis(dimethylamido) titanium (TDMAT) and electron exposures in a continuous  $\text{NH}_3$  reactive background gas.<sup>12</sup> The  $\text{NH}_3$  background gas at  $\sim 1 \text{ mTorr}$  greatly improved the purity of the TiN EE-ALD film presumably by providing  $\bullet\text{NH}_2$  and  $\bullet\text{H}$  radicals from electron impact dissociation of gas-phase  $\text{NH}_3$ .<sup>12</sup>

Silicon dioxide ( $\text{SiO}_2$ ) is one of the most common oxides.  $\text{SiO}_2$  is an important dielectric material in semiconductor devices.  $\text{SiO}_2$  is also used extensively as a transparent barrier coating material and as a reflective optical coating.  $\text{SiO}_2$  is a widely employed support for metals in heterogeneous catalysis. In addition,  $\text{SiO}_2$  is a common substrate for the deposition of many other thin films. Various ALD and chemical vapor deposition (CVD) methods have been developed previously for gas-phase  $\text{SiO}_2$  deposition.

Thermal  $\text{SiO}_2$  ALD has been demonstrated at high temperatures of 330–530 °C using  $\text{SiCl}_4$  and  $\text{H}_2\text{O}$  as the precursors.<sup>13,14</sup> Other studies have demonstrated thermal  $\text{SiO}_2$  ALD at  $>450$  °C using tris(dimethylamino)silane and  $\text{H}_2\text{O}_2$  as the precursors.<sup>15</sup> Catalyzed  $\text{SiO}_2$  ALD using various amines as the catalyst can reduce the  $\text{SiO}_2$  deposition temperature to 25 °C.<sup>16–18</sup> Plasma  $\text{SiO}_2$  ALD using precursors such as bis(diethylamino)silane together with  $\text{O}_2$  plasma can also lower the deposition temperature to 25–50 °C.<sup>19,20</sup> These plasma  $\text{SiO}_2$  ALD films may have high hydrogen content.<sup>21</sup>

Chemical vapor deposition (CVD) methods can also deposit  $\text{SiO}_2$  at low temperatures. Catalyzed  $\text{SiO}_2$  CVD has been demonstrated at 40–60 °C using  $\text{SiCl}_4$  and  $\text{H}_2\text{O}$  with an  $\text{NH}_3$  catalyst.<sup>22</sup> Plasma-enhanced CVD has also been performed at 40 °C using a tetraethyl orthosilicate and  $\text{O}_2$  plasma discharge.<sup>23</sup> Other demonstrations of plasma  $\text{SiO}_2$  CVD have been reported at temperatures from 100–350 °C.<sup>24,25</sup> Electron-assisted  $\text{SiO}_2$  CVD has also been achieved at temperatures as low as 150 °C when the electrons only interacted with gas phase reactants.<sup>3</sup> Lower temperatures down to room temperature were possible when the electrons could also interact with the substrate.<sup>26</sup>

This paper documents  $\text{SiO}_2$  EE-ALD at a low temperature of 35 °C using the HC-PES with  $\text{Si}_2\text{H}_6$  as the silicon precursor and  $\text{O}_3/\text{O}_2$  or  $\text{H}_2\text{O}$  as the oxygen reactant. This  $\text{SiO}_2$  EE-ALD is performed without the need for plasma activation, halide precursors, or catalysts. *In situ* spectroscopic ellipsometry (SE) measurements are employed to measure the  $\text{SiO}_2$  film thickness in real time. Because the HC-PES can deliver an electron beam into a chamber with a background gas present at pressures up to  $\sim 5 \text{ mTorr}$ ,  $\text{SiO}_2$  EE-ALD is also performed by codosing electrons and the oxygen reactants. In addition, many properties of the  $\text{SiO}_2$  EE-ALD films

are characterized and shown to be comparable with thermal  $\text{SiO}_2$  oxide films.

## II. EXPERIMENT

EE-ALD films were deposited in a V-shaped viscous-flow reactor with *in situ* spectroscopic ellipsometry (iSE, J. A. Woollam) capabilities at an angle of incidence of 70°. This V-shaped reactor is similar in design to a previously reported V-shaped reactor.<sup>27</sup> The reactor also had an HC-PES with electron optics to turn the electron beam to remove the sputtering flux from the output of the HC-PES as described previously.<sup>11</sup> The aperture of the HC-PES was  $\sim 28 \text{ cm}$  from the sample surface.

A computer-aided design (CAD) image of the main reactor body is shown in Fig. 1. Gate valves on the end of each arm of the V-shaped reactor were able to isolate the optical windows for spectroscopic ellipsometry. A gate valve also could isolate the hollow cathode and electron optics from the sample chamber. The chamber was pumped using either a turbomolecular pump (Pfeiffer HiPace 300C) or a mechanical pump (Alcatel 2010 C1). The turbomolecular pump was employed during the electron exposures. The mechanical pump was utilized for higher-pressure reactant exposures and during purging. A baratron capacitance monometer (MKS 121A) was also attached to the reactor to monitor pressure.

The sample was mounted to a metal plate with spring clips. The plate was able to slide in and out of the reactor for ease of sample transfer. The plate was also electrically isolated from the main reactor for accurate sample current measurements. The sample current was measured by a multimeter probe (Keithley, DMM7510 7.5 Digit Multimeter) connected to the sample stage.

The stage temperature was measured with a thermocouple probe inserted into the center of the stage. The temperature was defined by proportional integral derivative (PID) Eurotherm control (nanodac, Invensys) of four band heaters around the main chamber. The inlet arm, exhaust arm, and precursor lines of the reactor were also heated with additional band heaters, cartridge

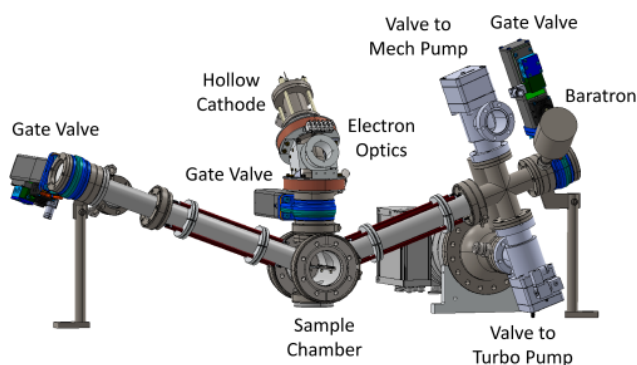


**FIG. 1.** V-shaped reactor with a hollow cathode plasma electron source (HC-PES) above the sample chamber. Gate valves at the end of each arm of the V-shaped reactor isolate the windows for spectroscopic ellipsometry. Pumping ports to either mechanical pump or turbomolecular pump connect through a four-way cross.

Downloaded from [http://pubs.aip.org/avs/jvst/article-pdf/doi/10.1116/6.0002726/18007981/042404\\_1\\_6.0002726.pdf](http://pubs.aip.org/avs/jvst/article-pdf/doi/10.1116/6.0002726/18007981/042404_1_6.0002726.pdf)

heaters, and fiberglass heat tapes that were controlled by voltage transformers (Variac).

The HC-PES delivered electrons to the sample surface. The hollow cavity of the HC-PES was biased at  $-350$  V relative to the bias grid voltage.<sup>11</sup> The bias grid voltage was biased relative to the ground and could be controlled to change the electron energy distribution. The bias grid voltage was variable between  $-50$  and  $-300$  V. Argon (Ar, 99.999%, Airgas) flow through the hollow cavity was 2.5 SCCM controlled by a mass flow controller (MFC) (MKS, 14 SCCM range).

SiO<sub>2</sub> EE-ALD was performed using the process sequence shown in Fig. 2. For SiO<sub>2</sub> EE-ALD, electrons were pulsed sequentially with Si<sub>2</sub>H<sub>6</sub> and either ozone (O<sub>3</sub>, 5 wt% in O<sub>2</sub>, LG-14 Corona Discharge Laboratory Ozone Generator) or de-ionized water. In the rest of this paper, the O<sub>3</sub>/O<sub>2</sub> exposure will be designated as O<sub>3</sub> for convenience. The process sequence using O<sub>3</sub> as the oxidation reactant is displayed in Fig. 2(a).

No gas, other than the Ar gas used to sustain the hollow cathode plasma, was flowing in the reactor during the electron beam pulse. During and after the O<sub>3</sub> (or H<sub>2</sub>O) and Si<sub>2</sub>H<sub>6</sub> exposures, nitrogen (N<sub>2</sub>, 99.999, Airgas) was used as an inert carrier gas and purge gas. The O<sub>3</sub> (or H<sub>2</sub>O) pressure transients were 0.5–1.0 Torr. The Si<sub>2</sub>H<sub>6</sub> dose pressure transients were 50 mTorr. N<sub>2</sub> flow was controlled by an MFC (MKS, 200 SCCM range) set to 100 SCCM. This N<sub>2</sub> flow resulted in a reactor base pressure of 0.7 Torr.

An alternate SiO<sub>2</sub> deposition process consisted of codosing electrons with the oxygen source, O<sub>3</sub> or H<sub>2</sub>O, followed by sequential dosing of Si<sub>2</sub>H<sub>6</sub>. The process sequence using O<sub>3</sub> as the

oxidation reactant codosing with electrons is displayed in Fig. 2(b). The codose process had N<sub>2</sub> flowing only during purging and the Si<sub>2</sub>H<sub>6</sub> exposure. The bias grid voltage was typically set to  $-300$  V for both the sequentially dosed and codosed processes.

Film growth was monitored with *in situ* spectroscopic ellipsometry (J. A. Woollam, iSE). SiO<sub>2</sub> films were deposited onto Si coupons with a native oxide. *Ex situ* spectroscopic ellipsometry with multiangle scan capabilities (J. A. Woollam, M-2000) was used to measure the SiO<sub>2</sub> film thickness and index of refraction using a Cauchy model.

*Ex situ* x-ray photoelectron spectroscopy (XPS, PHI 5600) depth profiling was used to measure the composition of the SiO<sub>2</sub> EE-ALD films. However, the Si:O ratio of the SiO<sub>2</sub> EE-ALD films could not be determined in the bulk due to preferential oxygen sputtering during depth profiling.<sup>28</sup> Atomic force microscopy (AFM, NX10, Park Systems) was employed to measure the surface roughness of the SiO<sub>2</sub> EE-ALD films. Grazing incidence x-ray diffraction (GIXRD, Bede D1, Jordan Valley Semiconductors) was used to characterize the crystallographic structure of the deposited films.

To assess film quality, SiO<sub>2</sub> EE-ALD films were etched in a diluted buffered oxide etch (dBOE) solution (5 ml buffered oxide etch, 6:1 from Sigma-Aldrich in 95 ml DI H<sub>2</sub>O). Etching in the dBOE solution occurred at 21 °C. Film thicknesses were measured periodically by SE. Films were precleaned with acetone, isopropyl alcohol, DI H<sub>2</sub>O rinse, and N<sub>2</sub> dry before being dipped in the dBOE solution for 10 s. Samples were then rinsed in a DI H<sub>2</sub>O bath for 1 min, followed by further de-ionized H<sub>2</sub>O rinsing before drying with N<sub>2</sub>. After this etching step, the film thickness was measured with multiangle SE. Subsequently, the films were dipped again in the dBOE solution for another 10 s and the process was repeated to progressively etch the SiO<sub>2</sub> film for a total of 40 s.

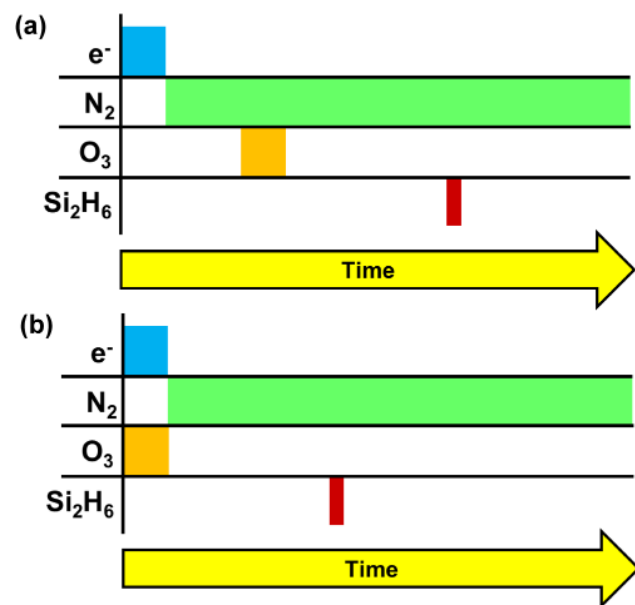


FIG. 2. Processing sequence for (a) SiO<sub>2</sub> EE-ALD based on sequential electron, O<sub>3</sub>, and Si<sub>2</sub>H<sub>6</sub> exposures and (b) SiO<sub>2</sub> EE-ALD based on codosing electron and O<sub>3</sub> exposures in sequence with Si<sub>2</sub>H<sub>6</sub> exposure. N<sub>2</sub> flow is continuous except during electron exposures.

### III. RESULTS AND DISCUSSION

#### A. SiO<sub>2</sub> EE-ALD using sequential electron beam, O<sub>3</sub>, and Si<sub>2</sub>H<sub>6</sub> exposures

SiO<sub>2</sub> EE-ALD films were grown at 35 °C using the process sequence shown in Fig. 2(a) with sequential electron beam, O<sub>3</sub>, and Si<sub>2</sub>H<sub>6</sub> exposures. Before SiO<sub>2</sub> EE-ALD, the sample was rinsed with acetone and IPA and dried with N<sub>2</sub> prior to loading. A 1 min e<sup>-</sup>|O<sub>3</sub> codose exposure was used to further clean the surface while under vacuum. One SiO<sub>2</sub> EE-ALD cycle consisted of an electron beam exposure for 3 s, purge for 5 s, O<sub>3</sub> exposure for 3 s, purge for 10 s, Si<sub>2</sub>H<sub>6</sub> exposure for 1 s, and purge for 15 s. There was an N<sub>2</sub> gas flow of 100 SCCM during the O<sub>3</sub> and Si<sub>2</sub>H<sub>6</sub> exposures and all purges.

An SiO<sub>2</sub> EE-ALD film was deposited on a Si sample at 35 °C using a  $-300$  V grid bias. Figure 3 shows the results for 500 SiO<sub>2</sub> EE-ALD cycles. The iSE measurements were started 8 s after the Si<sub>2</sub>H<sub>6</sub> exposures. The iSE measurements were conducted for 7 s. Consequently, the total purge time after the Si<sub>2</sub>H<sub>6</sub> exposures was 15 s. The SiO<sub>2</sub> EE-ALD growth is linear with time during the SiO<sub>2</sub> EE-ALD cycles with a cycle time of 37 s per cycle. A growth rate of 0.89 Å/cycle was observed with no nucleation delay.

The proposed surface processes during SiO<sub>2</sub> EE-ALD are as follows: The electron exposure forms active surface sites by electron

Downloaded from https://pubs.aip.org/avs/jvst/article-pdf/doi/10.1116/6.0002726/18007981/042404\_1\_6.0002726.pdf

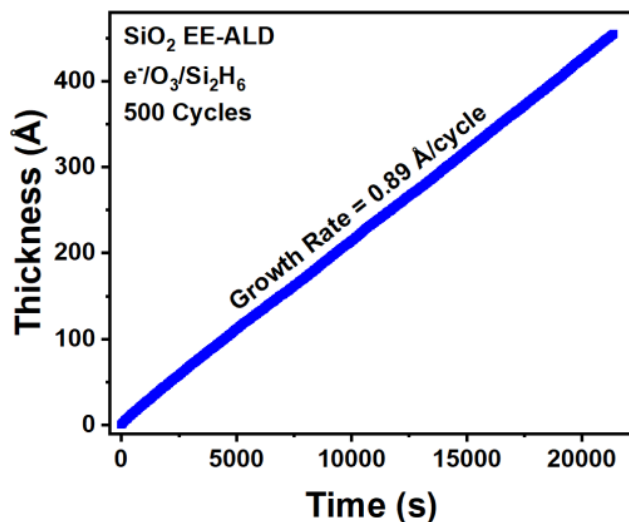


**FIG. 3.** SiO<sub>2</sub> thickness vs time during SiO<sub>2</sub> EE-ALD based on sequential electron, O<sub>3</sub>, and Si<sub>2</sub>H<sub>6</sub> exposures. The reaction sequence is electron beam exposure for 3 s, purge for 5 s, O<sub>3</sub> exposure for 3 s, purge for 10 s, Si<sub>2</sub>H<sub>6</sub> exposure for 1 s, and purge for 15 s. SiO<sub>2</sub> growth rate is 0.89 Å/cycle over 500 ALD cycles.

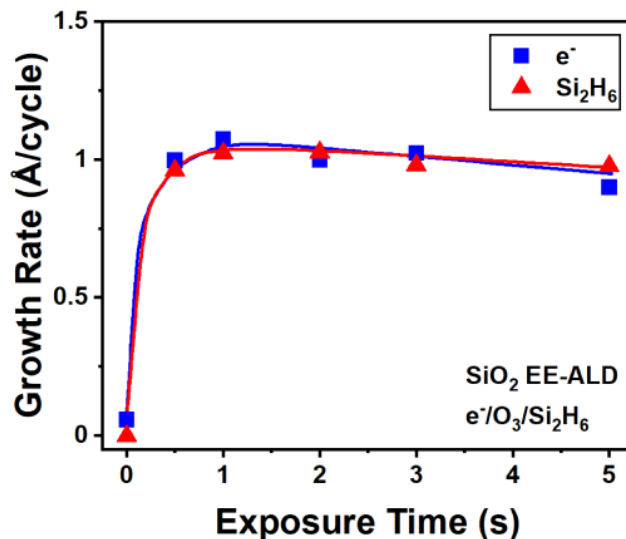


**FIG. 4.** SiO<sub>2</sub> EE-ALD growth rate vs electron or Si<sub>2</sub>H<sub>6</sub> exposure time based on sequential electron, O<sub>3</sub>, and Si<sub>2</sub>H<sub>6</sub> exposures. Si<sub>2</sub>H<sub>6</sub> exposure was fixed at 1 s when varying electron exposure. Electron exposure was fixed at 3 s when varying Si<sub>2</sub>H<sub>6</sub> exposure.

stimulated desorption (ESD). O<sub>3</sub> can then react with the active surface sites to form surface oxygen species. Subsequently, Si<sub>2</sub>H<sub>6</sub> can react with surface oxygen species or adsorb on active surface sites remaining from the ESD. The next electron exposure can then desorb hydrogen from SiH surface species resulting from Si<sub>2</sub>H<sub>6</sub> adsorption and form reactive Si dangling bond sites.<sup>8</sup> O<sub>3</sub> can then react with these reactive sites to oxidize the silicon surface species and form surface oxygen species. Si<sub>2</sub>H<sub>6</sub> can again react with surface oxygen species or adsorb on active surface sites remaining from the ESD.

The film thickness was mapped using multiangle *ex situ* SE. This mapping revealed a slight thickness gradient resulting from a minor misalignment of the electron beam from the center of the sample. The index of refraction from the *ex situ* multiangle SE Cauchy model fit was  $n = 1.457 + 0.00343/\lambda^2$  with a low mean squared error (MSE) of 3.190. In addition, AFM measurements of the surface roughness also confirmed smooth SiO<sub>2</sub> EE-ALD films with a root mean square (RMS) roughness of <2 Å.

The SiO<sub>2</sub> growth rate versus electron beam and Si<sub>2</sub>H<sub>6</sub> exposure times during SiO<sub>2</sub> EE-ALD using sequential electron, O<sub>3</sub>, and Si<sub>2</sub>H<sub>6</sub> exposures at 35 °C is shown in Fig. 4. Each growth rate point is an average of the last 20 cycles of a deposition period lasting 25 cycles. The nominal sequence for one SiO<sub>2</sub> EE-ALD cycle was: 3 s electron beam exposure, 5 s purge, 3 s O<sub>3</sub> exposure, 10 s purge, 1 s Si<sub>2</sub>H<sub>6</sub> exposure, and 15 s purge. The solid squares show the growth rate dependence on the electron beam exposure time with the Si<sub>2</sub>H<sub>6</sub> exposure time fixed at 1 s. The solid triangles show the growth rate dependence on the Si<sub>2</sub>H<sub>6</sub> exposure time with the electron beam exposure time fixed at 3 s. The SiO<sub>2</sub> EE-ALD growth rate saturates readily at the larger electron beam and Si<sub>2</sub>H<sub>6</sub> exposure times.

The SiO<sub>2</sub> EE-ALD growth rate was also examined versus the O<sub>3</sub> exposure time. However, SiO<sub>2</sub> film growth was observed even with no O<sub>3</sub> exposure time. SiO<sub>2</sub> film growth may occur with residual H<sub>2</sub>O desorbing from the chamber walls. The surface after the electron beam exposure contained dangling bonds that were highly reactive. Residual H<sub>2</sub>O may have been able to easily deposit on this reactive surface. In contrast, earlier experiments on Si EE-ALD using sequential Si<sub>2</sub>H<sub>6</sub> and electron exposures were performed under UHV conditions without using any oxygen sources during the course of the Si EE-ALD experiments.<sup>8</sup> Consequently, H<sub>2</sub>O partial pressures were extremely low and the Si EE-ALD films were deposited without oxygen impurities.

Additional experiments explored the dependence of SiO<sub>2</sub> EE-ALD on the bias grid voltage. The voltage was varied from -50 to -300 V. The SiO<sub>2</sub> EE-ALD growth rate versus bias grid voltage is shown in Fig. 5. Each data point is an average growth rate from deposition over 20 cycles with an SiO<sub>2</sub> EE-ALD cycle consisting of: 3 s electron beam exposure, 5 s purge, 3 s O<sub>3</sub> exposure, 10 s purge, 1 s Si<sub>2</sub>H<sub>6</sub> exposure, and 15 s purge. The lower growth rates at higher negative bias grid voltages may result from a small competitive etch or selective desorption of oxygen at these higher negative grid biases.

## B. SiO<sub>2</sub> EE-ALD using sequential electron beam, H<sub>2</sub>O, and Si<sub>2</sub>H<sub>6</sub> exposures

SiO<sub>2</sub> EE-ALD films were also grown at 35 °C with a -300 V grid bias using the process sequence shown in Fig. 2(a), where H<sub>2</sub>O was the oxygen source instead of O<sub>3</sub>. Figure 6 shows the results for 180 SiO<sub>2</sub> EE-ALD cycles. The sequence for one SiO<sub>2</sub> EE-ALD cycle

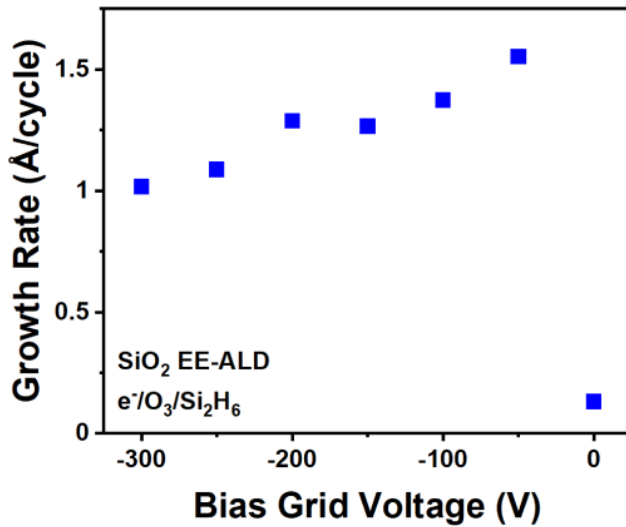


FIG. 5. SiO<sub>2</sub> EE-ALD growth rate vs bias grid voltage on the hollow cathode plasma electron source. SiO<sub>2</sub> EE-ALD was based on sequential electron, O<sub>3</sub>, and Si<sub>2</sub>H<sub>6</sub> exposures.

was 3 s electron beam exposure, 5 s purge, 3 s H<sub>2</sub>O exposure, 10 s purge, 1 s Si<sub>2</sub>H<sub>6</sub> exposure, and 15 s purge. The iSE measurements were collected 8 s after the Si<sub>2</sub>H<sub>6</sub> exposure. The SiO<sub>2</sub> EE-ALD growth is linear with time during the SiO<sub>2</sub> EE-ALD cycles with a cycle time

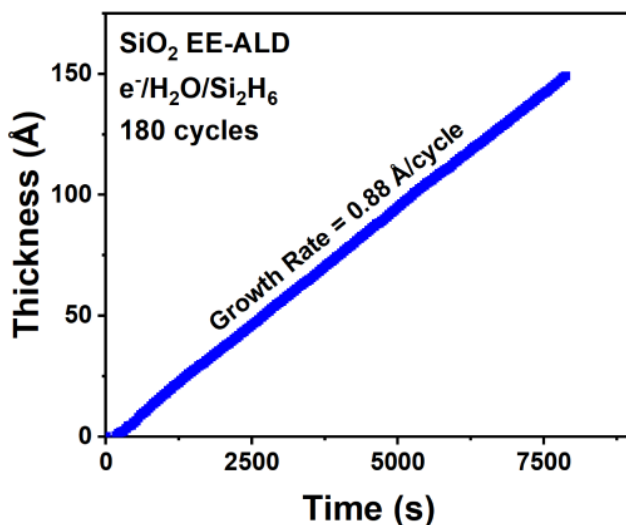


FIG. 6. SiO<sub>2</sub> thickness vs time during SiO<sub>2</sub> EE-ALD based on sequential electron, H<sub>2</sub>O, and Si<sub>2</sub>H<sub>6</sub> exposures. The reaction sequence is the electron beam exposure for 3 s, purge for 5 s, H<sub>2</sub>O exposure for 3 s, purge for 10 s, Si<sub>2</sub>H<sub>6</sub> exposure for 1 s, and purge for 15 s. The SiO<sub>2</sub> growth rate is 0.88 Å/cycle over 180 ALD cycles.

of 37 s per cycle. A growth rate of 0.88 Å/cycle was observed with no nucleation delay. The results in Figs. 3 and 6 are nearly equivalent. These results suggest that SiO<sub>2</sub> EE-ALD is not sensitive to the oxygen reactant. Since SiO<sub>2</sub> EE-ALD was observed even with no O<sub>3</sub> or H<sub>2</sub>O exposure, another possibility is that the background H<sub>2</sub>O dominated silicon oxidation in the SiO<sub>2</sub> EE-ALD process.

### C. SiO<sub>2</sub> EE-ALD using different reaction sequences

SiO<sub>2</sub> EE-ALD was also performed using a different reaction sequence where the electron exposure was performed after the oxygen reactant exposure. The results for SiO<sub>2</sub> EE-ALD using the sequence e<sup>-</sup>/Si<sub>2</sub>H<sub>6</sub>/O<sub>3</sub> are shown in Fig. 7. The reaction sequence was electron beam exposure for 3 s, purge for 5 s, Si<sub>2</sub>H<sub>6</sub> exposure for 1 s, purge for 15 s, O<sub>3</sub> exposure for 3 s, and purge for 10 s. Similar to the other SiO<sub>2</sub> EE-ALD growth curves shown in Figs. 3 and 6, the SiO<sub>2</sub> growth is linear and the nucleation of the SiO<sub>2</sub> film is immediate. This process sequence yielded a smaller growth rate of 0.68 Å/cycle. In comparison, a growth rate of 0.89 Å/cycle was obtained using the sequence e<sup>-</sup>/O<sub>3</sub>/Si<sub>2</sub>H<sub>6</sub> shown in Fig. 3. Likewise, a growth rate of 0.88 Å/cycle was obtained using the sequence e<sup>-</sup>/H<sub>2</sub>O/Si<sub>2</sub>H<sub>6</sub> shown in Fig. 6.

The SiO<sub>2</sub> growth rate was measured to be higher when the electron exposure was directly after the Si<sub>2</sub>H<sub>6</sub> exposure. This sequence may result in the desorption of the most hydrogen from SiH surface species.<sup>8</sup> This hydrogen desorption would result in the most reactive silicon dangling bond sites for the following O<sub>3</sub> exposure. Similar experiments were performed with the sequence e<sup>-</sup>/Si<sub>2</sub>H<sub>6</sub>/H<sub>2</sub>O. This sequence yielded an even smaller SiO<sub>2</sub> EE-ALD growth rate of 0.52 Å/cycle.

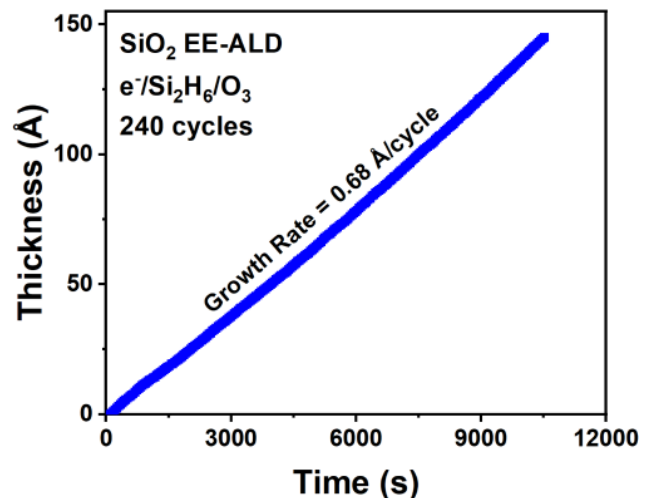


FIG. 7. SiO<sub>2</sub> thickness vs time during SiO<sub>2</sub> EE-ALD based on sequential electron, Si<sub>2</sub>H<sub>6</sub>, and O<sub>3</sub> exposures. The reaction sequence is the electron beam exposure for 3 s, purge for 5 s, Si<sub>2</sub>H<sub>6</sub> exposure for 1 s, purge for 15 s, O<sub>3</sub> exposure for 3 s, and purge for 10 s. The SiO<sub>2</sub> growth rate is 0.68 Å/cycle over 240 ALD cycles.

#### D. SiO<sub>2</sub> EE-ALD by codosing electron beam with oxygen reactant

Additional SiO<sub>2</sub> EE-ALD films were grown by codosing the electron beam and either O<sub>3</sub> or H<sub>2</sub>O together with Si<sub>2</sub>H<sub>6</sub> using the process sequence shown in Fig. 2(b). These SiO<sub>2</sub> EE-ALD films were also grown at 35 °C with a −300 V grid bias. Figure 8 shows the results for 195 SiO<sub>2</sub> EE-ALD cycles using O<sub>3</sub> as the oxygen reactant for electron beam/O<sub>3</sub> codosing. During the codose exposures, the oxygen source pressure was ≤5 mTorr. The codose cycle consisted of a 3 s codose e<sup>−</sup>|O<sub>3</sub> exposure (or e<sup>−</sup>|H<sub>2</sub>O exposure), 10 s purge, 1 s Si<sub>2</sub>H<sub>6</sub> exposure, and 15 s purge. The iSE measurements were collected 8 s after the Si<sub>2</sub>H<sub>6</sub> exposure.

The SiO<sub>2</sub> EE-ALD growth with electron beam/O<sub>3</sub> codosing in Fig. 8 is linear with time during the SiO<sub>2</sub> EE-ALD cycles with a cycle time of 29 s per cycle. A growth rate of 0.73 Å/cycle was observed with no nucleation delay. Similar results were obtained when performing SiO<sub>2</sub> EE-ALD using H<sub>2</sub>O as the oxygen reactant for electron beam/H<sub>2</sub>O codosing. There was no nucleation delay and the growth rate was 0.59 Å/cycle.

During codosing of the electron beam with the oxygen reactant, the electron beam can interact with the oxygen reactant in the gas phase. Electron impact could lead to the dissociation of O<sub>3</sub> or H<sub>2</sub>O. O<sub>2</sub> is the main component of the O<sub>3</sub>/O<sub>2</sub> exposure. The cross section for O<sub>2</sub> dissociation by an electron impact at 200 eV is 3 × 10<sup>−17</sup> cm<sup>2</sup>.<sup>29</sup> The cross section for H<sub>2</sub>O dissociation by an electron impact at 300 eV is 1 × 10<sup>−16</sup> cm<sup>2</sup>.<sup>30</sup> Similar cross sections are also observed for the ionization of O<sub>2</sub> or H<sub>2</sub>O.<sup>30,31</sup> The radical or ion species from this electron impact could adsorb on the growing SiO<sub>2</sub> film. However, the lower growth rate for SiO<sub>2</sub> EE-ALD when codosing the electron beam with the oxygen reactant indicates that

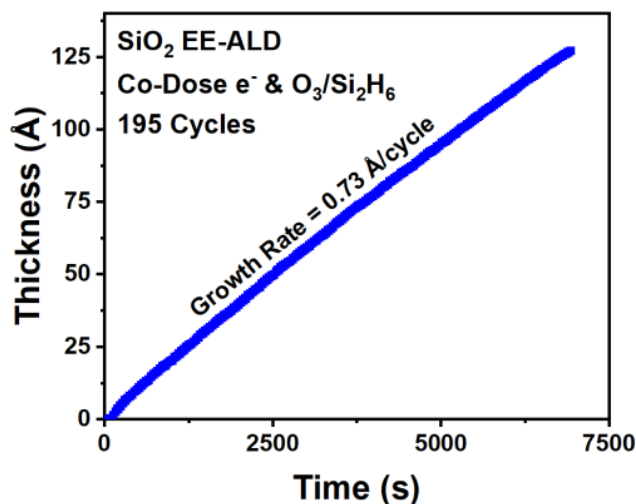


FIG. 8. SiO<sub>2</sub> thickness vs time during SiO<sub>2</sub> EE-ALD based on codosing electron and O<sub>3</sub> exposures in sequence with Si<sub>2</sub>H<sub>6</sub> exposures. The codose cycle was codose e<sup>−</sup>|O<sub>3</sub> exposure for 3 s, purge for 10 s, Si<sub>2</sub>H<sub>6</sub> exposure for 1 s, and purge for 15 s. The SiO<sub>2</sub> growth rate is 0.73 Å/cycle over 195 ALD cycles.

the possible adsorption of these reactive species does not increase the growth rate for SiO<sub>2</sub> EE-ALD.

The self-limiting nature of the SiO<sub>2</sub> growth versus codosing electrons/O<sub>3</sub> and Si<sub>2</sub>H<sub>6</sub> was also explored using the process sequence in Fig. 2(b). The SiO<sub>2</sub> growth rate versus e<sup>−</sup>|O<sub>3</sub> and Si<sub>2</sub>H<sub>6</sub> exposure times at 35 °C is shown in Fig. 9. The nominal process conditions were 3 s e<sup>−</sup>|O<sub>3</sub> (or e<sup>−</sup>|H<sub>2</sub>O) codose, 10 s purge, 1 s Si<sub>2</sub>H<sub>6</sub> dose, and 15 s purge. Each data point represents the growth rate determined from an average of 20 cycles. The solid squares show the growth rate dependence on the codose e<sup>−</sup>|O<sub>3</sub> exposure time with the Si<sub>2</sub>H<sub>6</sub> exposure time fixed at 1 s. The solid triangles show the growth rate dependence on the Si<sub>2</sub>H<sub>6</sub> exposure time with the codose e<sup>−</sup>|O<sub>3</sub> exposure time fixed at 3 s. N<sub>2</sub> at 100 SCCM was used as the inert carrier gas during the Si<sub>2</sub>H<sub>6</sub> exposure and the purges. No N<sub>2</sub> was flowing during the electron beam codosing with O<sub>3</sub> or H<sub>2</sub>O.

Figure 9 shows that the SiO<sub>2</sub> growth rate saturates with increasing exposure time of either the e<sup>−</sup>|O<sub>3</sub> exposure or the Si<sub>2</sub>H<sub>6</sub> exposure. In these experiments, the SiO<sub>2</sub> growth rate was self-limiting at 0.55–0.60 Å/cycle. These growth rates are slightly lower than the growth rate of 0.73 Å/cycle measured for the results in Fig. 8. The growth rates may be lower because they were determined using only 20 SiO<sub>2</sub> EE-ALD cycles. Similar experiments were performed to explore the self-limiting nature of SiO<sub>2</sub> growth versus codosing e<sup>−</sup>|H<sub>2</sub>O and Si<sub>2</sub>H<sub>6</sub>. These experiments also revealed that the SiO<sub>2</sub> growth was self-limiting versus the codosing e<sup>−</sup>|H<sub>2</sub>O exposures and the Si<sub>2</sub>H<sub>6</sub> exposures.

#### E. SiO<sub>2</sub> growth rates, refractive indices, and etch rates for different process conditions

The SiO<sub>2</sub> EE-ALD growth rates for the different process conditions are given in Table I. The highest growth rates of 0.88–0.89

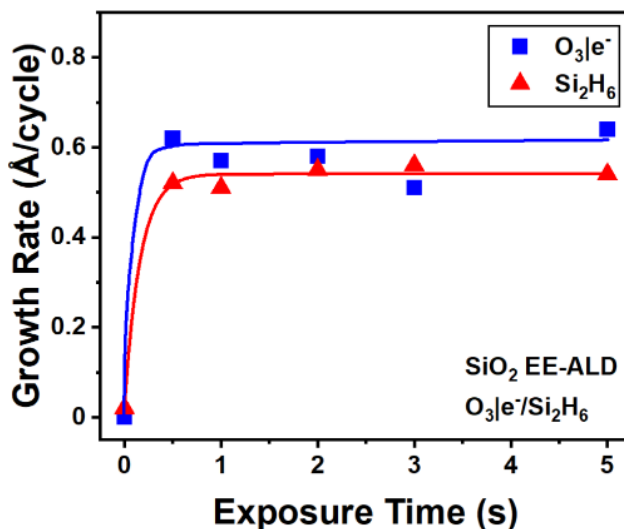


FIG. 9. SiO<sub>2</sub> EE-ALD growth rate vs exposure time based on codosing electron and O<sub>3</sub> exposures in sequence with Si<sub>2</sub>H<sub>6</sub> exposures. Si<sub>2</sub>H<sub>6</sub> exposure is fixed at 1 s when codosing electron and O<sub>3</sub> exposures. Codosing e<sup>−</sup>|O<sub>3</sub> exposure is fixed at 3 s when varying Si<sub>2</sub>H<sub>6</sub> exposure.

**TABLE I.** Growth rate, refractive index, and dilute buffered oxide etch (dBOE) rates for various SiO<sub>2</sub> EE-ALD films. The SiO<sub>2</sub> EE-ALD films are indicated by a sequential (s) or codose (c) reaction sequence. The refractive index and dBOE rate for a wet thermal oxide film with a thickness of 300 nm is given for comparison.

Sample	Growth rate (Å/cycle)	Refractive index	dBOE (Å/s)
s. e <sup>-</sup> /O <sub>3</sub> /Si <sub>2</sub> H <sub>6</sub>	0.89	1.457	2.166 ± 0.019
s. e <sup>-</sup> /H <sub>2</sub> O/Si <sub>2</sub> H <sub>6</sub>	0.88	1.443	2.378 ± 0.109
s. e <sup>-</sup> /Si <sub>2</sub> H <sub>6</sub> /O <sub>3</sub>	0.68	1.445	2.670 ± 0.129
s. e <sup>-</sup> /Si <sub>2</sub> H <sub>6</sub> /H <sub>2</sub> O	0.52	1.438	2.316 ± 0.137
c. e <sup>-</sup> &O <sub>3</sub> /Si <sub>2</sub> H <sub>6</sub>	0.73	1.417	2.377 ± 0.052
c. e <sup>-</sup> &H <sub>2</sub> O/Si <sub>2</sub> H <sub>6</sub>	0.59	1.437	2.786 ± 0.004
Wet thermal SiO <sub>2</sub>	—	1.447	0.943 ± 0.068

Å/cycle were observed for the sequential electron beam, oxygen reactant, and Si<sub>2</sub>H<sub>6</sub> exposures as shown in Fig. 2(a). The lowest SiO<sub>2</sub> EE-ALD growth rates of 0.52–0.73 Å/cycle were observed for the process sequence where the electron exposures were after the oxygen reactant exposure or when the electron beam and oxygen reactant were codosed as shown in Fig. 2(b).

The refractive indices were also measured for each process condition after SiO<sub>2</sub> EE-ALD using *ex situ* multiangle SE. The refractive index values were similar for all the process conditions. The refractive index was measured to be  $n_{\infty} = 1.44 \pm 0.02$ . This refractive index is nearly identical to the refractive index measured for the SiO<sub>2</sub> film prepared by thermal oxidation of a silicon wafer using H<sub>2</sub>O. These wet SiO<sub>2</sub> thermal oxide films were prepared by University Wafer at a process temperature of 900–1050 °C.

SiO<sub>2</sub> films were analyzed with *ex situ* XPS to characterize film purity. XPS depth profile elemental analysis showed high-quality SiO<sub>2</sub> films as deposited by EE-ALD. The carbon atomic percent in the bulk of the films was below the detection limit of the instrument. Nitrogen was present in the bulk of the film at ~1 at. %. The remaining 99 at. % of the film contained only silicon and oxygen. Based on the ratio of Si at. % and O at. %, the films were SiO<sub>1.2</sub>. These apparently substoichiometric films may be caused by preferential O sputtering.<sup>28</sup> The Si 2p binding energy was 102.4 eV as expected for SiO<sub>2</sub>. In addition, *ex situ* GIXRD was used to analyze the crystallographic structure of the SiO<sub>2</sub> EE-ALD films. The SiO<sub>2</sub> films were determined to be amorphous.

The dilute buffered oxide etch rates were also measured for all of the SiO<sub>2</sub> EE-ALD films. The etch rates are shown in Fig. 10 and also included in Table I. Each SiO<sub>2</sub> EE-ALD film had a starting thickness of ~125 Å. The wet thermal oxide had a starting thickness of 3248 Å. The SiO<sub>2</sub> films were etched in the dilute buffered oxide etch (dBOE) solution for 10 s at a time. The SiO<sub>2</sub> films were etched for a total time of 40 s. The SiO<sub>2</sub> film thicknesses were evaluated by spectroscopic ellipsometry measurements after etching for 20, 30, and 40 s. The SiO<sub>2</sub> film thicknesses versus etch time were fit to obtain the SiO<sub>2</sub> etch rates. The Cauchy values for the fits to the ellipsometry results were kept constant versus thickness and between the samples.

The dBOE rates for all the SiO<sub>2</sub> EE-ALD films were consistent across the various process sequences. The lowest SiO<sub>2</sub> etch rate was

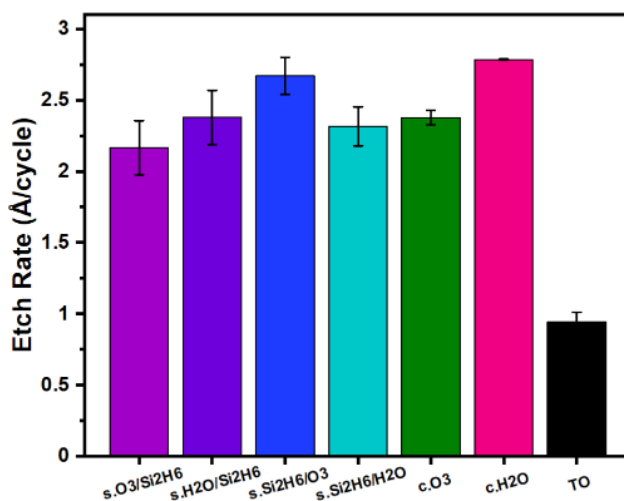


**FIG. 10.** Etch rate of SiO<sub>2</sub> EE-ALD films in dilute buffered oxide etch solution for all SiO<sub>2</sub> EE-ALD process conditions. SiO<sub>2</sub> thermal oxide (TO) is also included for comparison. Sequence (s) or codosing (c) conditions are indicated and electron exposures are not designated explicitly. Si<sub>2</sub>H<sub>6</sub> exposures are also not designated explicitly for the codosing conditions.

2.166 ± 0.019 Å/s for the e<sup>-</sup>/O<sub>3</sub>/Si<sub>2</sub>H<sub>6</sub> process sequence. The highest SiO<sub>2</sub> etch rate was 2.786 ± 0.004 Å/s for the codose e<sup>-</sup> and H<sub>2</sub>O/Si<sub>2</sub>H<sub>6</sub> process sequence. The etch rate for the wet thermal oxide was 0.943 ± 0.068 Å/s. SiO<sub>2</sub> EE-ALD films have slightly faster etch rates than wet thermal oxide SiO<sub>2</sub> films. However, these slightly larger etch rates are consistent with high-quality SiO<sub>2</sub> films for all SiO<sub>2</sub> EE-ALD processes.

## F. EE-ALD on insulating SiO<sub>2</sub> substrates

These studies revealed that electron currents on insulating SiO<sub>2</sub> substrates can grow SiO<sub>2</sub> EE-ALD films. This behavior may be surprising because the initial expectation is that primary electron currents on an insulating substrate may charge the substrate negatively. This negative charge would then establish a voltage that would repel additional electron current and prevent EE-ALD. However, if the secondary electron yield,  $\delta$ , is greater than unity, the sample would emit more secondary electrons than impinge on the sample from the primary electron beam. These competing primary and secondary electron fluxes would establish a positive charge on the sample surface.<sup>32</sup> This positive charge would create a voltage that pulls back enough secondary electrons to maintain a constant low surface charge.<sup>32,33</sup>

For a continuous electron current, the insulator with  $\delta > 1$  would charge to a voltage where the number of secondary electrons having enough energy to escape would equal the number of incident primary electrons.<sup>32</sup> Under these conditions, there is no additional charging and SiO<sub>2</sub> EE-ALD can proceed without complication. Only the primary incident electron energy may be increased slightly resulting from the positive voltage determined by the constant low surface charge on the insulating SiO<sub>2</sub> substrate.<sup>33</sup>

Measurements for SiO<sub>2</sub> reveal that  $\delta$  is greater than 1 for primary electron energies from  $\sim 100$  to 1000 eV.<sup>34,35</sup> These secondary electron yields greater than unity allow EE-ALD to be performed on SiO<sub>2</sub> and other insulating substrates.

In addition to maintaining a low constant surface charge, the high secondary electron yields from SiO<sub>2</sub> may also influence the surface chemistry during SiO<sub>2</sub> EE-ALD. Earlier studies of the effect of low energy electron bombardment on O<sub>2</sub> oxidation of silicon observed the largest enhancement of silicon oxidation at electron energies that produced the highest secondary electron yields.<sup>36</sup> A previous demonstration of SiO<sub>2</sub> electron-induced CVD using Si<sub>2</sub>H<sub>6</sub> and O<sub>2</sub> as the reactants also observed larger SiO<sub>2</sub> growth rates at electron energies that yielded the largest secondary electron yields.<sup>26</sup>

#### IV. CONCLUSIONS

This study explored the ability of electrons to enhance SiO<sub>2</sub> ALD at low temperatures using disilane (Si<sub>2</sub>H<sub>6</sub>) and either ozone (O<sub>3</sub>/O<sub>2</sub>) or water (H<sub>2</sub>O) as the reactants. SiO<sub>2</sub> electron-enhanced ALD (EE-ALD) was demonstrated at 35 °C by exposing the sample to sequential electron, oxygen reactant, and Si<sub>2</sub>H<sub>6</sub> exposures. SE measurements revealed that the SiO<sub>2</sub> EE-ALD films nucleated rapidly and deposited SiO<sub>2</sub> films linearly versus the number of EE-ALD cycles on silicon coupons with a native oxide. The SiO<sub>2</sub> EE-ALD growth rates were independent of the oxygen reactant. The measured SiO<sub>2</sub> EE-ALD growth rates were 0.89 Å/cycle using O<sub>3</sub>/O<sub>2</sub> and 0.88 Å/cycle using H<sub>2</sub>O. The SiO<sub>2</sub> growth rates were also self-limiting at higher electron and Si<sub>2</sub>H<sub>6</sub> exposures. The SiO<sub>2</sub> EE-ALD films could also be grown by codosing the electron and oxygen reactant exposures in sequence with the Si<sub>2</sub>H<sub>6</sub> exposure.

The SiO<sub>2</sub> EE-ALD films could be deposited on conducting or insulating substrates. The SiO<sub>2</sub> EE-ALD films were grown on either conducting silicon wafers or insulating SiO<sub>2</sub> films. The secondary electron yield can explain the ability to perform EE-ALD on insulating substrates. SiO<sub>2</sub> EE-ALD may occur on insulating SiO<sub>2</sub> films because the secondary electron yield for SiO<sub>2</sub> at electron energies of  $\sim 100$ – $300$  eV is greater than unity. When the secondary electron yield is greater than unity, the SiO<sub>2</sub> film charges positive during electron exposure and then pulls back secondary electrons to maintain a small positive bias of a few volts.

The measured properties of the SiO<sub>2</sub> EE-ALD films were comparable with thermal SiO<sub>2</sub> oxide films. The refractive indices of the SiO<sub>2</sub> EE-ALD films were similar at  $n = 1.44 \pm 0.02$  for the various process conditions. This refractive index is equivalent to the refractive index of a thermal SiO<sub>2</sub> oxide film formed by the oxidation of a silicon wafer using H<sub>2</sub>O. For wet etching in dilute buffered oxide etch solutions, all the SiO<sub>2</sub> EE-ALD films yielded etch rates that were only slightly higher than the etch rate of a thermal SiO<sub>2</sub> oxide film. The ability to deposit SiO<sub>2</sub> on both conducting and insulating substrates at low temperatures will lead to new possibilities for SiO<sub>2</sub> deposition on thermally sensitive substrates.

#### ACKNOWLEDGMENTS

This research was funded by Samsung Semiconductor, Inc. The authors thank Sanghoon Ahn from Samsung for technical discussions and samples. The authors also acknowledge Kenneth

Smith and Don David from the University of Colorado Integrated Instrument Development Facility for their construction and maintenance of the HC-PES and help with computer interfacing.

#### AUTHOR DECLARATIONS

##### Conflict of Interest

The authors have no conflicts to disclose.

##### Author Contributions

**Jonas C. Gertsch:** Conceptualization (equal); Data curation (lead); Formal analysis (lead); Investigation (lead); Methodology (equal); Writing – original draft (lead); Writing – review & editing (supporting). **Zachary C. Sobell:** Conceptualization (equal). **Andrew S. Cavanagh:** Resources (lead). **Harsono Simka:** Conceptualization (equal); Project administration (supporting); Supervision (supporting); Writing – review & editing (supporting). **Steven M. George:** Conceptualization (equal); Funding acquisition (lead); Methodology (equal); Project administration (lead); Supervision (lead); Writing – review & editing (lead).

##### DATA AVAILABILITY

The data that support the findings of this study are available within the article.

##### REFERENCES

- 1 R. D. Ramsier and J. T. Yates, *Surf. Sci. Rep.* **12**, 246 (1991).
- 2 F. Bozso and P. Avouris, *Phys. Rev. B* **38**, 3943 (1988).
- 3 L. R. Thompson, J. J. Rocca, K. Emery, P. K. Boyer, and G. J. Collins, *Appl. Phys. Lett.* **43**, 777 (1983).
- 4 I. Utke, P. Hoffmann, and J. Melngailis, *J. Vac. Sci. Technol. B* **26**, 1197 (2008).
- 5 W. F. van Dorp and C. W. Hagen, *J. Appl. Phys.* **104**, 081301 (2008).
- 6 H. B. Profijt, S. E. Potts, M. C. M. van de Sanden, and W. M. M. Kessels, *J. Vac. Sci. Technol. A* **29**, 050801 (2011).
- 7 J. K. Sprenger, A. S. Cavanagh, H. Sun, K. J. Wahl, A. Roshko, and S. M. George, *Chem. Mater.* **28**, 5282 (2016).
- 8 J. K. Sprenger, H. Sun, A. S. Cavanagh, and S. M. George, *J. Vac. Sci. Technol. A* **36**, 01A118 (2017).
- 9 J. K. Sprenger, H. Sun, A. S. Cavanagh, A. Roshko, P. T. Blanchard, and S. M. George, *J. Phys. Chem. C* **122**, 9455 (2018).
- 10 Z. C. Sobell, A. S. Cavanagh, and S. M. George, *J. Vac. Sci. Technol. A* **37**, 060906 (2019).
- 11 Z. C. Sobell, A. S. Cavanagh, D. R. Boris, S. G. Walton, and S. M. George, *J. Vac. Sci. Technol. A* **39**, 042403 (2021).
- 12 Z. C. Sobell and S. M. George, *Chem. Mater.* **34**, 9624 (2022).
- 13 J. W. Klaus, A. W. Ott, J. M. Johnson, and S. M. George, *Appl. Phys. Lett.* **70**, 1092 (1997).
- 14 O. Sneh, M. L. Wise, A. W. Ott, L. A. Okada, and S. M. George, *Surf. Sci.* **334**, 135 (1995).
- 15 B. B. Burton, S. W. Kang, S. W. Rhee, and S. M. George, *J. Phys. Chem. C* **113**, 8249 (2009).
- 16 Y. Du, X. Du, and S. M. George, *Thin Solid Films* **491**, 43 (2005).
- 17 J. W. Klaus and S. M. George, *Surf. Sci.* **447**, 81 (2000).
- 18 J. W. Klaus, O. Sneh, and S. M. George, *Science* **278**, 1934 (1997).
- 19 G. Dingemans, C. A. A. van Helvoirt, D. Pierreux, W. Keuning, and W. M. M. Kessels, *J. Electrochem. Soc.* **159**, H277 (2012).
- 20 S. E. Potts, H. B. Profijt, R. Roelofs, and W. M. M. Kessels, *Chem. Vap. Deposition* **19**, 125 (2013).

- <sup>21</sup>M. Putkonen *et al.*, *Thin Solid Films* **558**, 93 (2014).
- <sup>22</sup>J. W. Klaus and S. M. George, *J. Electrochem. Soc.* **147**, 2658 (2000).
- <sup>23</sup>S. C. Deshmukh and E. S. Aydil, *Appl. Phys. Lett.* **65**, 3185 (1994).
- <sup>24</sup>G. Lucovsky, P. D. Richard, D. V. Tsu, S. Y. Lin, and R. J. Markunas, *J. Vac. Sci. Technol. A* **4**, 681 (1986).
- <sup>25</sup>C. Martinet, V. Paillard, A. Gagnaire, and J. Joseph, *J. Non-Cryst. Solids* **216**, 77 (1997).
- <sup>26</sup>K. Nakano, T. Horie, and H. Sakamoto, *Jpn. J. Appl. Phys., Part 1* **35**, 6570 (1996).
- <sup>27</sup>M. Junige and S. M. George, *J. Vac. Sci. Technol. A* **39**, 023204 (2021).
- <sup>28</sup>D. H. Kim, G. H. Lee, S. Y. Lee, and D. H. Kim, *J. Cryst. Growth* **286**, 71 (2006).
- <sup>29</sup>P. C. Cosby, *J. Chem. Phys.* **98**, 9560 (1993).
- <sup>30</sup>M. Y. Song, H. Cho, G. P. Karwasz, V. Kokoouline, Y. Nakamura, J. Tennyson, A. Faure, N. J. Mason, and Y. Itikawa, *J. Phys. Chem. Ref. Data* **50**, 023103 (2021).
- <sup>31</sup>E. Krishnakumar and S. K. Srivastava, *Int. J. Mass Spectrom. Ion Process.* **113**, 1 (1992).
- <sup>32</sup>H. J. Hopman, H. Alberda, I. Attema, H. Zeijlemaker, and J. Verhoeven, *J. Electron. Spectrosc. Relat. Phenom.* **131**, 51 (2003).
- <sup>33</sup>J. Cazaux and P. Lehuede, *J. Electron. Spectrosc. Relat. Phenom.* **59**, 49 (1992).
- <sup>34</sup>G. F. Dionne, *J. Appl. Phys.* **46**, 3347 (1975).
- <sup>35</sup>J. J. Fijol, A. M. Then, G. W. Tasker, and R. J. Soave, *Appl. Surf. Sci.* **48–49**, 464 (1991).
- <sup>36</sup>R. R. Kunz and T. M. Mayer, *J. Vac. Sci. Technol. B* **5**, 427 (1987).